


Unconventional reentrant quantum Hall effect in a HgTe/CdHgTe double quantum wellM. V. Yakunin,^{1,*} S. S. Krishtopenko,² W. Desrat,² S. M. Podgornykh,¹ M. R. Popov,¹
V. N. Neverov,¹ S. A. Dvoretzky,³ N. N. Mikhailov,³ F. Teppé,² and B. Jouault²¹*M. N. Miheev Institute of Metal Physics UB RAS, 620137 Ekaterinburg, Russia*²*Laboratoire Charles Coulomb, UMR 5221 Centre National de la Recherche Scientifique,
University of Montpellier, F-34095 Montpellier, France*³*Institute of Semiconductor Physics SB RAS, 630090 Novosibirsk, Russia* (Received 13 November 2018; revised 22 September 2020; accepted 22 September 2020; published 9 October 2020)

We report on the observation of an unconventional structure of the quantum Hall effect (QHE) in a *p*-type HgTe/Cd_{1-x}Hg_xTe double quantum well (DQW) consisting of two HgTe layers of critical thickness. The observed QHE is a reentrant function of magnetic field between two $i = 2$ states (plateaus at $\rho_{yx} = h/ie^2$) separated by an intermediate $i = 1$ state in the shape of a flat-top peak placed on the remarkably long $i = 2$ plateau. This anomalous $i = 1$ peak separates two different regimes: (i) a traditional QHE at relatively low fields corresponding to a small density of mobile holes p_s , and (ii) a high-field QHE with a 2-1 plateau-plateau transition corresponding to a much larger p_s . The high-field part is strongly sensitive to external influences such as gate voltages, in contrast to the low-field part, which is much less responsive. We explain the observed behavior by analyzing the calculated trajectories of the Fermi level $E_F(B)$ between hole-like and electron-like Landau levels (LLs). At low fields, E_F is captured by the lateral maximum (LM) of the valence subband, and only holes in the center of the Brillouin zone contribute to QHE, while holes in the LM are inactive. In contrast, at fields above the reentry, E_F rises significantly higher than LM, approaching the zero-mode LLs, and all holes come into play in QHE. At intermediate fields, the reentrance is caused by a combination of two factors in the specific energy spectrum of this DQW: (i) the superposition of an electron-like LL on hole-like LLs and (ii) the stabilizing influence of the LM reservoir on $E_F(B)$.

DOI: [10.1103/PhysRevB.102.165305](https://doi.org/10.1103/PhysRevB.102.165305)**I. INTRODUCTION**

The quantum Hall effect (QHE) manifests most typically as a stair-like sequence of plateaus in the Hall magnetoresistivity (MR) $\rho_{xy}(B)$ located at its monotonically increasing values $\rho_{xy}(B) = h/ie^2$ for integer or fractional filling factors i [1]. This picture is disturbed by a nonmonotonic reentrant behavior of $\rho_{xy}(B)$ for the integer QHE (RIQHE) in some special cases: for a two-subband conductivity due to Landau level (LL) or subband mixing [2]; in a traditional double quantum well (DQW) under tilted magnetic fields [3], where certain QH states are repeatedly destroyed as a function of the parallel-field component B_{\parallel} due to an oscillating behavior of the tunneling gap; and in the excited LLs of samples with record high mobility at extra-low temperatures [4–9] due to repeated transitions between the collective quantum liquid and pinned quantum solid bubble states [10,11]. In this paper, we demonstrate a distinct RIQHE appearing in a complex energy spectrum of the HgTe DQW at helium temperatures and for moderate mobilities that may be basically explained without recourse to the collective nature of the electronic phases.

The uniqueness of the energy structure of the HgTe QW and its strong dependence on the well thickness [12] make this material suitable to construct various kinds of nontrivial energy spectra in a system of two HgTe layers separated by a thin

Cd_{1-x}Hg_xTe barrier, i.e., in a HgTe/CdHgTe DQW [13,14]. Different applications were predicted for this structure [15,16] which is also an opportunity to study fundamental phenomena in new conditions [17]. Experimentally, several remarkable novel features were revealed in quantum magnetotransport on HgTe DQWs with relatively thick HgTe layers, like reentrant sign-alternating QH states, the possibility to enlarge and regulate the band overlap, and the enhanced zero filling factor state [13]. In the present study, we found that probably the most unusual features of quantum magnetotransport appear in a *p*-type HgTe/CdHgTe DQW when the thickness of the HgTe layers is close to the critical value $d \approx d_c = 6.3\text{--}6.5$ nm, i.e., when a Dirac energy spectrum is formed in a single HgTe layer [12]. In this case, a RIQHE is revealed [18] that has indications of switching between two states with different densities of mobile holes. The only analog we know of such a kind of “switching” between different net carrier densities with magnetic field was reported for a multi-quantum-well structure made within a GaAs parabolic quantum well [19], where the effect was attributed to a spatial redistribution of electrons between different wells. In our case, we show that the observed “switching” is an inherent property of the DQW energy spectrum.

II. SAMPLES AND MEASUREMENTS

DQW structures were grown by molecular-beam epitaxy on a (013)-orientated GaAs substrate above a series of

*yakunin@imp.uran.ru

ZnTe and CdTe buffer layers. The DQW consists of two HgTe layers with a thickness $d = 6.5 \pm 0.2$ nm separated by a 3 ± 0.1 nm $\text{Cd}_x\text{Hg}_{1-x}\text{Te}$ barrier with $x = 0.71$. There is no intentional doping. The layer widths were controlled by single-wavelength ellipsometry during the growth [20]. Magnetoabsorption studies of similar structures confirmed that ellipsometry gives the correct estimation of the layer thicknesses [21,22]. Hall bar devices were then shaped by photolithography. The overall size of the Hall bar is 3×1 mm². For some Hall bars, a top gate was fabricated with parylene as an insulator and aluminum as a gate electrode. Indium was directly soldered at the contact pads of the devices to ensure the formation of ohmic contacts to both layers of the DQW. We measured the longitudinal and Hall MRs $\rho_{xx}(B)$ and $\rho_{yx}(B)$ at temperatures down to 0.26 K and in magnetic fields up to 13 T. The measurements were performed on two ungated and two gated samples obtained from the same DQW growth (No. 150218). The four Hall bars gave identical results, and for clarity, we will present the results obtained mainly with one of the gated samples.

III. ENERGY SPECTRUM

The DQW parameters have been chosen to reproduce the so-called “bilayer graphene” (BG) phase described in Ref. [14]. The band dispersion of each of the two HgTe/CdHgTe QWs taken separately is a Dirac cone, because the nominal thickness of the QWs corresponds to the critical thickness d_c at which the gap disappears.

Numerically, the energy dispersion of the DQW was calculated by an 8-band $\mathbf{k} \times \mathbf{p}$ method, including the influence of elastic strain. The details of the calculation can be found in Ref. [14]. The band dispersion of the DQW is shown in Fig. 1 with the spatially quantized levels of a single HgTe QW shown in the inset. The dispersion of a single QW is characterized by two groups of levels—those of the heavy-hole (HH) nature and of the electron-like carriers (E)—that move quickly toward each other with increasing layer thickness d . At a critical thickness d_c , the extreme levels in both series intersect and the Dirac spectrum is formed at this meeting point. Specific features of the energy spectrum in a DQW made of these HgTe layers are due to that. The E levels of single layers are strongly tunnel-coupled when joined into the DQW, which is contrary to the HH levels, where the interlayer coupling becomes significant only with an increase in k : see the main panel of Fig. 1. In the DQW energy spectrum, we denote the upper and lower subbands, which are split off from the corresponding level of the single quantum well, by the superscript (¹ and ²).

The gapless isotropic energy dispersion of the DQW is remarkably similar to the one of natural BG as it consists of two touching parabolas formed by subbands $HH1^1$ and $HH1^2$ and of two spaced parabolas: $E1^1$ and $E1^2$. Differences with respect to natural BG are also noticed. In particular, a lateral maximum (LM) appears around $k \simeq 0.4$ nm⁻¹ in subbands $HH1^1$ and $E1^1$. This LM is associated with a very flat dispersion and hence yields a high density of states (DOS). Side maxima in the valence band of single HgTe/CdHgTe QWs are also predicted theoretically and have been observed experimentally by magnetotransport [23–26].

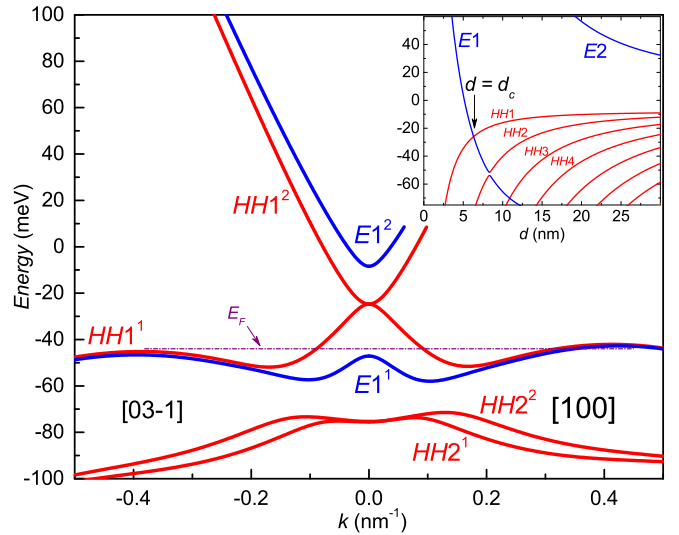


FIG. 1. Energy spectrum of the DQW under study, if its potential profile is symmetrical. Inset: Spatial levels of a single QW as a function of the layer thickness d . The upper index on the main figure (¹ or ²) means the first or second split-off subband in a DQW originating from the corresponding level of a single well. The Fermi level E_F is drawn for the case of no gate.

The estimated deviations in the energy spectrum and in the positions of the LLs induced by technological errors of the layer thicknesses are within ± 3 meV. Therefore, they do not introduce a radical restructuring of $E(k)$ or the LL scheme. Qualitative changes in the spectrum will occur only in the case of opposite deviations of the thicknesses of the two QWs. In this case, a gap of less than 2 meV opens between the HH branches due to the thus-induced DQW asymmetry. This gap also appears (or is modified) if an electrical field is applied perpendicular to the layers, which causes a slope in the DQW potential profile [14].

IV. EXPERIMENTAL RESULTS

A. Magnetoresistivities

Natural BG has an unconventional QHE with an anomalous sequence of quantum Hall plateaus, $i = \pm 4, \pm 8, \pm 12, \dots$. One may wonder how the QHE will manifest in our “artificial BG”. Figure 2(a) shows the Hall MR $\rho_{yx}(B)$ at different gate voltages V_g and at a temperature $T = 260$ mK, when the magnetic field B is swept between 0 T and 1.7 T. At $B < 0.2$ T, the classical Hall effect is apparent and the slope yields hole densities varying between $p_s \simeq 0.38 \times 10^{15}$ m⁻² at $V_g = -1$ V and $p_s \simeq 0.27 \times 10^{15}$ m⁻² at $V_g = 1.7$ V. The variation of the hole density with V_g is very slow, $dp_s/dV_g \simeq 0.037 \times 10^{15}$ m⁻²/V, and is incomparably smaller than the estimate for the geometric capacitance, $(1/e)dQ/dV_g \simeq 0.6 \times 10^{15}$ m⁻²/V. Such a deviation has already been evidenced for single HgTe QWs, cf. Ref. [24], and has been attributed to the coexistence of two types of hole states: those in the central and lateral maxima of the valence subband. The latter have a much lower mobility, and they do not contribute to quantum magnetotransport.

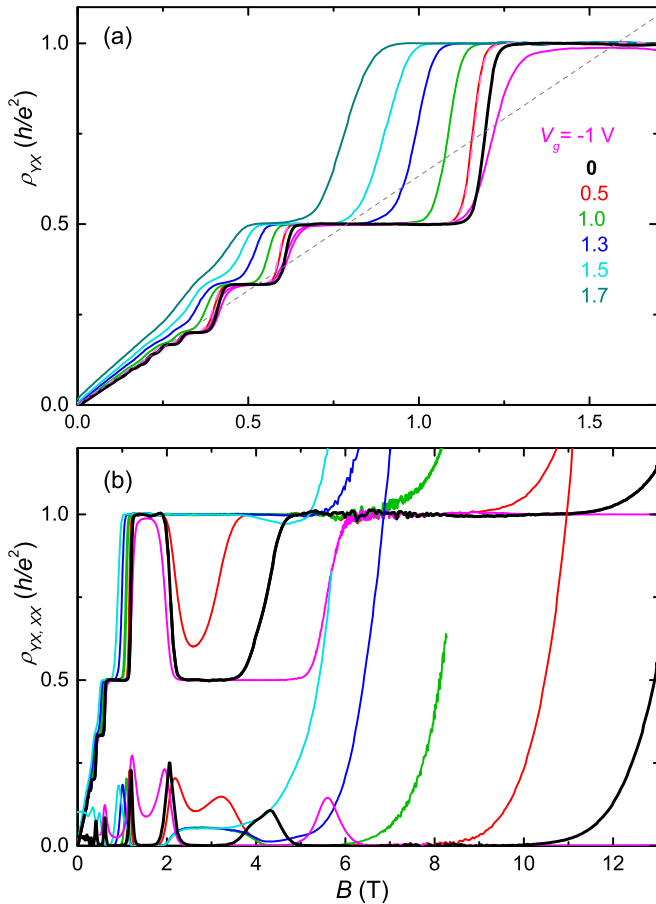


FIG. 2. (a) Transverse magnetoresistivity $\rho_{yx}(B)$ at $T = 260$ mK, for $B = 0$ –1.7 T and V_g varying from -1 V to 1.7 V; (b) transverse and longitudinal magnetoresistivities $\rho_{yx}(B)$ and $\rho_{xx}(B)$ on an extended magnetic field range, $B = 0$ –13 T, for the same temperature and gate voltages V_g as in (a).

The sample resistivity as a function of gate voltage passes through a maximum around $V_g = 3$ V thus indicating the charge neutrality point (CNP). Simultaneously the Hall resistivity changes its sign indicating the transition to the n -type conductivity at high V_g .

At higher fields a traditional succession of QH plateaus $\rho_{yx} = h/ie^2$ is observed in Fig. 2(a), with i varying from about 8 down to 1 as B increases up to 1.5 T. The extrapolation of the classical Hall resistivity crosses QH plateaus near their centers, as evidenced by the dashed black line for $V_g = 0$. The QHE does not reveal any intriguing features here.

However, Fig. 2(b) shows that at still higher magnetic fields the ρ_{yx} behavior becomes unusual. For gate voltages $V_g \leq 0.5$ V, the $i = 1$ plateau collapses around $B \simeq 1.8$ –2 T, and ρ_{yx} returns to the $i = 2$ QH plateau. Subsequently, at higher magnetic fields $B \simeq 3$ –6 T, ρ_{yx} increases again and the $i = 1$ plateau reappears. At even higher fields, both ρ_{yx} and ρ_{xx} increase and diverge. Assuming that the magnetic field at which the second plateau-plateau transition (PPT) $i = 2 \rightarrow 1$ takes place corresponds to the filling factor $i = 1.5$, this gives the hole density $p_s \simeq 1.66 \times 10^{15} \text{ m}^{-2}$ at $V_g = 0$, about four times larger than that obtained at low B . The reaction of the p_s value found in this way to the applied V_g is $dp_s/dV_g \simeq$

$(0.52 \pm 0.05) \times 10^{15} \text{ m}^{-2}/\text{V}$, which is close to the estimated geometric capacitance and 14 times stronger than that in the low-field regime.

The Fermi level E_F position for $p_s = 1.66 \times 10^{15} \text{ m}^{-2}$ is drawn in Fig. 1 where it is almost aligned with LM. This suggests that the observed RIQHE of the $i = 2$ plateau may be somehow linked to the population of LM.

B. Calculation of the LLs

To explain the observed features of magnetoresistivity, we extended calculations by means of the 8-band $\mathbf{k} \times \mathbf{p}$ Hamiltonian to obtain LLs. We use the axial approximation [14] by keeping the in-plane rotation symmetry and omitting all warping terms resulting from cubic symmetry of zinc-blende semiconductors, bulk inversion asymmetry (BIA) of the unit cell in bulk zinc-blende crystals, and interface inversion asymmetry (IIA) due to anisotropy of chemical bonds at the QW interfaces. We note that it is rotational symmetry that allows one to introduce conventional LL indices in narrow-gap QW systems. As the electric field \mathcal{E} applied perpendicular to the QW plane preserves the in-plane rotational symmetry, it can be taken into account within the axial approximation as well.

In natural BG, \mathcal{E} is an important parameter as it opens a gap in the energy dispersion due to introduction of asymmetry into the potential profile. Similarly, so introduced asymmetry opens a gap in the spectrum of our DQW, as demonstrated in Ref. [14].

As revealed from the magnetoabsorption experiments [27], there is a gap of about 3 meV in the spectrum of ungated samples cut from the same wafer from the same source as our samples. This gap exceeds the value that can be caused by the difference in the QW widths within the technological errors. Therefore, this gap is most likely due to the residual electric field. For a given gap, the local electric field should be of the order of $\mathcal{E} \simeq 10$ kV/cm over a barrier width of 3 nm. That is why we start analyzing our results at zero and low gate voltages, comparing them with the LL pattern calculated for the asymmetric DQW profile, with asymmetry caused by the tentative value of $\mathcal{E} = 10$ kV/cm; see Fig. 3. This induced gap is visible at $B = 0$ and is retained with increasing field between the $n = -2$ LLs. Other LLs emerge from both the upper and lower edges of the gap.

In the overall picture, several LLs with specific behavior are seen. These are the so-called “zero-mode LLs” with quantum numbers $n = 0, -1$, and -2 known in a single HgTe QW [28,29]. Two of these LLs, with $n = -2$ (shown as gray solid lines), follow parallel lines when B increases and go slightly downward. Another LL, with $n = 0$ (shown as a thick red line), emerges from the lower subband $E1^1$. It undergoes a local anticrossing with another $n = 0$ LL but goes up continuously and finally crosses the two $n = -2$ LLs.

C. Landau levels and lateral maximum

At low energies $E \leq -42$ meV in the valence subband, a dense grid of LLs appears: Fig. 3(a). These LLs have a nonmonotonic dispersion. They originate from the top of the $HH1^1$ and $E1^1$ subbands at $B = 0$ T and first they move downward, then upward, and finally go downward again. This

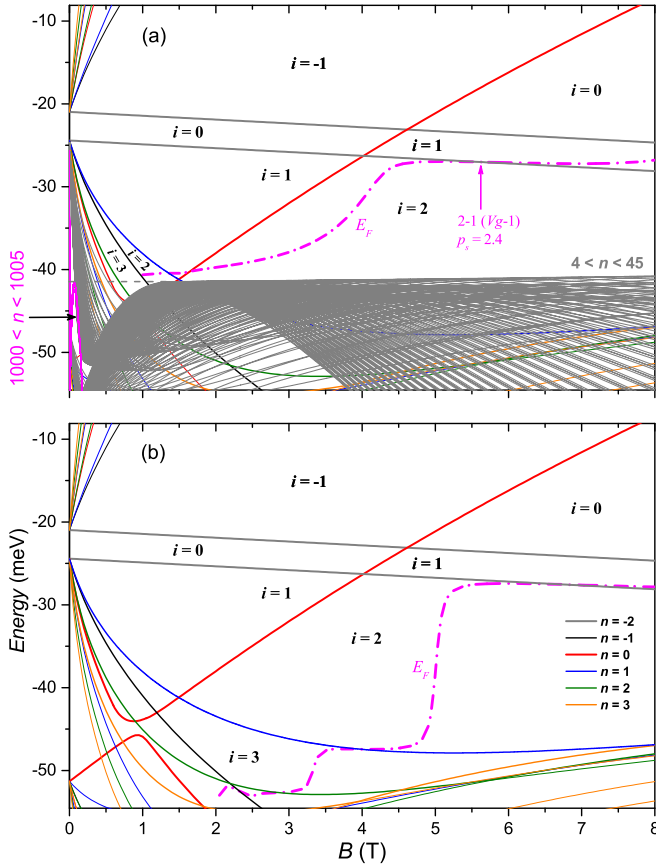


FIG. 3. (a) The Landau-level fan chart of the DQW with asymmetrical potential profile due to a perpendicular electric field (as found experimentally for zero and negative V_g). Each region delimited by the LLs is labeled by the index i defining the expected transverse conductivity $\sigma_{xy} = ie^2/h$ (i is negative for electrons). The Fermi energy $E_F(B)$, calculated for $p_s = 2.4 \times 10^{15} \text{ m}^{-2}$ (experimentally found for $V_g = -1 \text{ V}$), is indicated as a dot-dashed magenta line. (b) Same as (a), but with only a reduced number of LLs taken into account. The trace for $E_F(B)$ found in this case is incorrect since the influence of LM is lost.

nonmonotonic behavior of the LLs is imposed by the shape of subbands and by the Onsager relation $\mathcal{A}(E_n) = 2\pi(n + \gamma)eB_n/h$, where γ is a phase shift and \mathcal{A} is the area in the k space enclosed by the classical orbital of the LL of index n and energy E_n . In a semiclassical picture, assuming axial symmetry for clarity (it does not change the validity of the result), E_n is associated with a trajectory in the two-dimensional cross section of constant energy along the considered subband, $HH1^1(k)$ or $E1^1(k)$, and the corresponding area is $\mathcal{A} = \pi k^2$. As the Onsager relation imposes that this trajectory must enclose an area which is proportional to B , we get $E_n(B) = HH1^1(k = aB^{1/2})$ with $a \propto \sqrt{n + \gamma}$. Thus, the nonmonotonic variation of the LL energy vs B reflects the nonmonotonic energy variation of the $HH1^1$ subband vs k . The same reasoning is valid for the lower valence subbands. However, we emphasize that the behavior of the zero-mode LLs cannot be explained quasiclassically. They do not obey the Onsager relation.

It follows from the quasiclassical approach that LLs with different n reach a fixed energy at fields $B_n \propto 1/n$. Thus, the

$E_n(B)$ curves are compressed along the B axis with increasing n . This corresponds to the LM energy as well, and the maxima of these LLs follow a line of constant energy till $B = 0$ with $n \rightarrow \infty$. It means that an infinite array of LLs fills as a dense grid the entire range of weak fields below the LM energy till $B \rightarrow 0$ for $n \rightarrow \infty$, thus forming something like a LL band (considering that individual LLs are hardly resolved in such a dense grid). This is confirmed by the digital calculations of a fragment for $n = 1000$ – 1005 presented in Fig. 3(a). For $n \leq 45$, the DOS in our calculations is underestimated below $B \simeq 1 \text{ T}$. The dashed gray horizontal line in the weak-field part of Fig. 3(a) indicates the direction in which the upper edge of this LL band should follow.

D. Fermi level as a function of field and its stabilization at the LM energy

To explain the observed features of QHE, we calculated the trajectories along which the Fermi level moves with the field between the LLs: $E_F(B)$. It was done for finite DOS in LLs (we used a Lorentzian with a fixed half-width of 0.5 meV) for a set of constant values of the total carrier density in the sample, considering the hole or electron type of the carriers in a LL. We assumed in calculations that the hole-like (electron-like) LLs are those moving down (up) in energy with increasing field regardless of what subband they come from. This consideration is confirmed by the fact that the LLs shift in the same direction on approaching the sample edge [30,31] as they do in magnetic fields; see Eqs. (64) and (66) in Ref. [32], and also Ref. [30]. Correspondingly, we consider the contribution to p_s , and to $\rho_{yx}(B)$ or conductivity $\sigma_{xy}(B)$, as positive from the hole-like and negative from the electron-like LLs.

We take into account only the geometric capacitance of the system, neglecting the quantum capacitance. A constant V_g then corresponds to a constant carrier density p_s in the DQW. To fulfill this condition, p_s was calculated as a difference between the overall hole density in the hole-like LLs above $E_F(B)$ and the electron density in the electron-like LLs below it [13,33,34].

When the nature of conductivity in the LLs is known, be it hole-like or electron-like, each gap between LLs can be labeled with an integer value i indicating the difference between the number of populated hole-like LLs and the electron-like ones. It is these numbers i that must correspond to the quantum Hall effect plateau numbers in the experiment, when $E_F(B)$ falls into this gap.

The transition point between different i states corresponds to the intersection of the calculated $E_F(B)$ trajectory with the delocalized state at the center of the LL separating the corresponding gaps. Taking into account the finite width of the DOS at the LL makes it possible to estimate the transition field more accurately than in the simplified approach for the δ -shaped DOS peaks. In the latter case, it is assumed by default that the transition occurs at a half-integer value of i . Thus, for the case of no gate such a simplified estimation for the high-field 2-1 PPT yields, for $i = 1.5$, $p_s = 1.66 \times 10^{15} \text{ m}^{-2}$, while it is somewhat larger for our case of finite DOS: $p_s = 1.9 \times 10^{15} \text{ m}^{-2}$.

When the finite DOS in LLs is considered, one can correctly evaluate the role of LM in quantum magnetotransport.

We believe that the observed unusual experimental behavior can be explained by properties of the DQW energy spectrum, first of all, by a stabilizing influence of the LM on the $E_F(B)$, due to a high DOS in it. To see this, a sufficiently large number of LLs should be included in the calculations ($n \leq 45$ in our case) to reproduce the dense grid of LLs below the LM energy and hence the associated high DOS.

If too few LLs are taken into account, this grid of LLs becomes sparse, the DOS in the valence subband is drastically underestimated, and the $E_F(B)$ curve is traditional, crossing LLs periodically in $1/B$ throughout the entire field range, see Fig. 3(b), which is in stark contrast with our experiment. On the contrary, with a sufficiently fully built dense LL grid of LM, the calculated behavior of $E_F(B)$ becomes completely different. In this case, when $E_F(B)$ tends to go down in energy, passing with decreasing field to LLs with larger numbers, it falls into the vicinity of LM and, as a result of a very high local DOS here, the decrease of $E_F(B)$ slows down and it even stops in the tails of LLs of this dense grid. One can say that $E_F(B)$ is stabilized near the LM energy in the weak-field range.

E. The reservoir-like behavior at low fields

Even if the high DOS of the LM is not well reproduced below 1 T by our calculations, we can draw some conclusions.

The $E_F(B)$ shown in Fig. 3(a) makes the weak-field $i = 2 \rightarrow 1$ transition at $B \simeq 1.4$ T through the $n = 1$ LL that corresponds to the central maximum in the second valence subband in this range of fields. The position of this crossing formally corresponds to $i = 1.5$ that yields an apparent carrier density $1.5 \times eB/h \approx 0.5 \times 10^{15} \text{ m}^{-2}$, which is much lower than the carrier density $p_s = 2.4 \times 10^{15} \text{ m}^{-2}$ (taken from the experimental high-field 2-1 PPT for $V_g = -1$ V) used in the calculation of the whole $E_F(B)$ trace. But it is much closer to the data of the classical Hall effect on the same experimental curve. In this state, a large number of holes have been absorbed by the LLs in the dense grid of LM. These LLs remain below E_F and are poorly resolved in the dense grid, so they do not cause any quantum Hall features. Therefore, the structure of QHE in the weak-field part is formed exclusively by holes of the central maximum and gives the density of these very carriers.

Such a behavior may be compared to the ‘‘reservoir’’ model for QHE, in which the reservoir absorbs a part of carriers excluding them from magnetotransport [35,36]. However, unlike previous works, this ‘‘reservoir’’ in our case is not connected with the surrounding of the quasi-2D structure [37,38] and is not due to some in-plane inhomogeneity [39]. Instead, the reservoir is induced by the LM, which is an integral part of the conductive layer [40].

F. Unusually wide $i = 2$ plateau and QHE at high fields

With increasing field, $E_F(B)$ moves upward in its evolution to LLs with lower numbers and, finally, reaches the uppermost hole-like LLs with $n = -2$; see Fig. 3(a). These two zero-mode LLs behave in a completely different way with respect to the lower hole-like LLs. They move down linearly and very slowly with the field, and as a result they become much higher in energy than all the other hole LLs,

even at relatively weak fields. Therefore, a large gap is formed between the lower $n = -2$ LL and the other hole-like LLs below. As $E_F(B)$ progressively moves up with the field in this wide $i = 2$ gap, it goes far from the LM energy, so that LM becomes depopulated by holes. When the two upper LLs are spaced from the other hole-like LLs and LM by much greater distance than their broadening Γ , the usual $1/B$ periodicity of quantum magnetotransport is restored at high fields, and now all holes participate in the formation of QHE. Hence, the total hole density p_s is manifested in the high-field $i = 2 \rightarrow 1$ transition.

Thus, the calculation of $E_F(B)$ for the correct picture of LLs and the finite DOS at LLs makes it possible to explain why only holes from the central maximum manifest in the QHE of the HgTe DQW at low fields, while the QHE at higher fields corresponds to the true total constant density of holes. The unusually wide $i = 2$ state is obtained in calculations due to the prolonged transition between these two regimes, when $E_F(B)$ gradually leaves the high-DOS energy range next to LM, moving with increasing field within a wide gap through the high DOS area of the LM LL tails to the topmost LLs. The main specificity of this process here is that not a single LL, but many LLs in a dense LL grid of LM are simultaneously depleted by increasing the field.

Returning to the reservoir model, it should be noted that when explaining the anomalously wide *first* plateau observed in a single QW in previous works [26,35,38,39], it was only *assumed* that the phenomenon is associated with the field-dependent transfer of current carriers from a certain reservoir to a conducting monolayer, while other mechanisms that can delay the transition of the first plateau to a dielectric state can also influence the process. On the contrary, the abnormally wide $i = 2$ state observed in our case in the DQW is automatically derived from the calculations yielding a high-field 2-1 PPT, from which definitely follows a p_s value significantly larger than that obtained in the weak fields. Thus, we formally get *direct* evidence of an increase in the density of mobile carriers at high fields.

G. High-field $i = 1$ plateau as a proof of the DQW potential asymmetry

Having established the correspondence between the labels of the gaps between LLs in the calculated picture of LLs and the QH plateau numbers, we obtain direct proof of the initial (ungated) DQW asymmetry. This follows from the existence of a high-field $i = 1$ QH plateau for $V_g < \sim 1.5$ V. Indeed, at high fields this plateau corresponds to the gap between two $n = -2$ LLs, while for a symmetric DQW potential profile these two zero-mode hole-like $n = -2$ LLs must coincide [14]. The gap between the two *HH1* subbands, and between the two zero-mode $n = -2$ LLs, occurs only when the DQW becomes asymmetric.

Thus, we confirm the conclusion of the magnetoabsorption studies of this DQW [27] that the two $n = -2$ LLs are split. The physical origin of the asymmetry causing this splitting is yet unclear. Most likely, this could be due to a built-in perpendicular electric field caused by an uneven distribution of charges inside the barriers or the fixed charges in the interfaces and on the surface.

H. Mechanism of the RIQHE

The anomalous behavior of the zero-mode $n = 0$ LL emerging from the central maximum of the lower valence subband $E1^1$ creates a nontrivial situation, which leads to the observed unconventional structure of the QHE. The combination of a LL fan chart descending from the central maximum of the upper valence subband $HH1^1$, an anomalous upward movement of the $n = 0$ LL, and the LM stabilizing effect on $E_F(B)$, Fig. 3(a), leads to that, when increasing the field from small values, the calculated $E_F(B)$ successively crosses the regions corresponding to $i = 3, 2, 1, 2$, and 1.

The observed RIQHE is induced by the weak-field $i = 1$ region between LLs which has the shape of a base-up triangle surrounded by two gaps of $i = 2$. Remarkably, the lower corner of this inverted quasi-triangle is located just above the LM energy. The Fermi level E_F , stabilized by the proximity to LM, cuts off the lower corner of this triangle and enters the $i = 1$ region within a limited range of fields, thus causing the appearance of the flat-top ρ_{yx} peak observed in Fig. 2 with a $i = 1$ plateau surrounded by two $i = 2$ plateaus.

Evolution of the reentrance with V_g is shown more in detail in the $\sigma_{xy}(B, V_g)$ color map, Fig. 4(a), where it is compared with the calculated picture of LLs for the asymmetrical DQW with the superposed $E_F(B)$ trajectories for a set of V_g values below 1.3 V. A stabilizing influence of LM on $E_F(B)$ is expressed on the map in the vertical boundaries of the $i = 1$ strip in the range of $B = 1\text{--}2$ T and $V_g < 1$ V. Only at the lowest values of $V_g = -2.5$ V this vertical strip narrows, reflecting the approach of the $E_F(B)$ to the lower vertex of the $i = 1$ triangular gap.

The left border of this vertical strip starts moving to the lower fields for $V_g > 1$ V indicating that for these low enough p_s densities the Fermi level starts moving up leaving the high-DOS area next to LM.

The reentrant behavior of QHE disappears when, at $V_g > 0.5$ V, the $E_F(B)$ trajectories on their moving up with V_g no longer enter the high-field $i = 2$ gap: Fig. 4(b).

It should be noted that a somewhat similar RIQHE was observed in Refs. [12] and [31] in a single HgTe layer of the same 6.5 nm width, but between the $i = 1$ phase and the $i = 0$ insulating states: $i = 0 \rightarrow 1 \rightarrow 0$, so it was a flat-bottom structure in $\rho_{yx}(B)$ with a restricted $i = 1$ plateau at its bottom and with sides going to infinity. This picture is upside down when compared to our flat-top peak with the $i = 1$ plateau on its top. Their flat-bottom structure was also interpreted as being due to intersecting electron-like and hole-like LLs.

I. Anticrossing in the $i = 1$ region

With an increase in V_g from 0 to +1 V, $E_F(B)$ is pushed upward from the high-field $i = 2$ gap, as is seen in Fig. 4(b) when switching from the black dash-dot curve to the green one. In the intermediate case, $E_F(B)$ will enter the $i = 2$ gap only in a narrow range of fields, as shown in Fig. 4(a) by a short light-yellow horizontal line at 2–3 T for $V_g = +0.5$ V. This is manifested in a significantly weakened transition back to the $i = 2$ state, when it is displayed only as a minimum on the $i = 1$ plateau: see Fig. 2(b) for this V_g . Finally, this minimum disappears for $V_g > 0.5$ V, when E_F will be completely in the $i = 1$ gap.

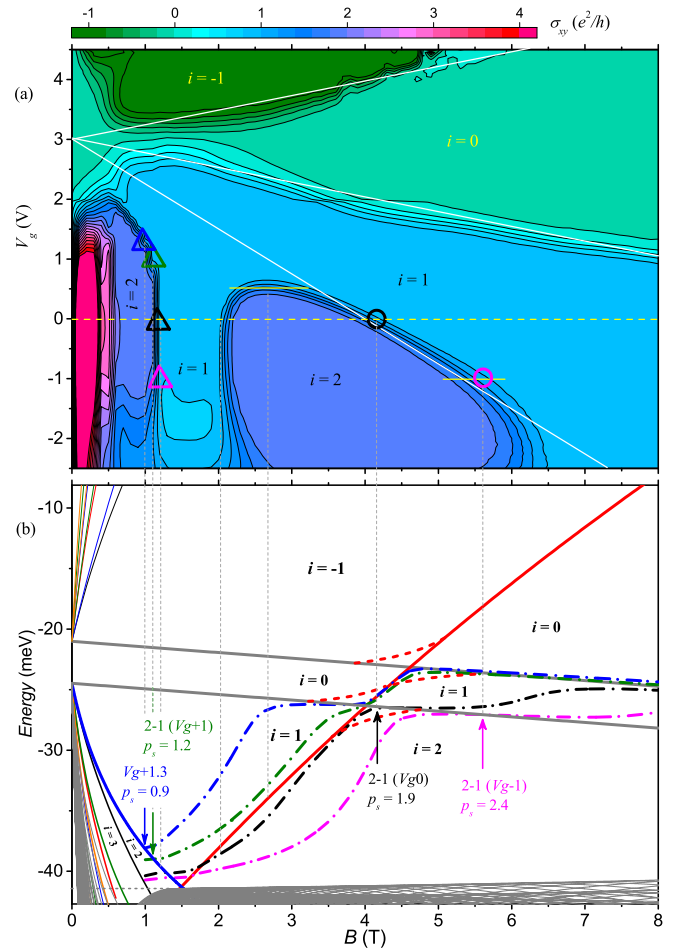


FIG. 4. (a) Color map of the transverse conductivity $\sigma_{xy}(B, V_g)$ at $T = 260$ mK. The white lines are expected plateau-to-plateau transitions. The triangles and circles are the positions of the first and second $i = 2 \rightarrow 1$ transitions, respectively, as deduced from panel (b). (b) Zoom of the LL fan chart reported for asymmetrical DQW potential from Fig. 3, put in relation with the σ_{xy} map. The Fermi levels $E_F(B)$ for carrier densities $p_s = 2.4 \times 10^{15} \text{ m}^{-2}$ ($V_g = -1$ V), $1.9 \times 10^{15} \text{ m}^{-2}$ ($V_g = 0$), $0.9 \times 10^{15} \text{ m}^{-2}$ (1 V), and $0.5 \times 10^{15} \text{ m}^{-2}$ (1.3 V) are reported as dot-dashed colored lines. The thick dashed red lines are illustrations of possible anticrossings.

To be more precise, E_F should be located in two sectors of this gap in this case, as seen in Fig. 4(b). Surprisingly, the passage of $E_F(B)$ through the constriction between the two sectors does not manifest in $\rho_{yx}(B)$, although some elevation appears in $\rho_{xx}(B)$ between $B = 2$ and 4 T for $V_g = 1\text{--}1.5$ V: see Fig. 2(b) and the map Fig. 5, where the elevation is indicated by the green arrow. From our experiments in tilted magnetic fields (see below) it is distinct that $\rho_{xx}(B)$ in its minima is more sensitive to the details of the LL picture than the plateaus in $\rho_{yx}(B)$.

These data mean that in fact there is an anticrossing between the zero-mode $n = -2$ and $n = 0$ LLs, so that a continuous connection is formed between the two sectors of the $i = 1$ gap, as shown schematically by the red short-dashed curves in Fig. 4(b) around the expected intersections of these LLs. In this case, the elevation in $\rho_{xx}(B)$ indicates not the

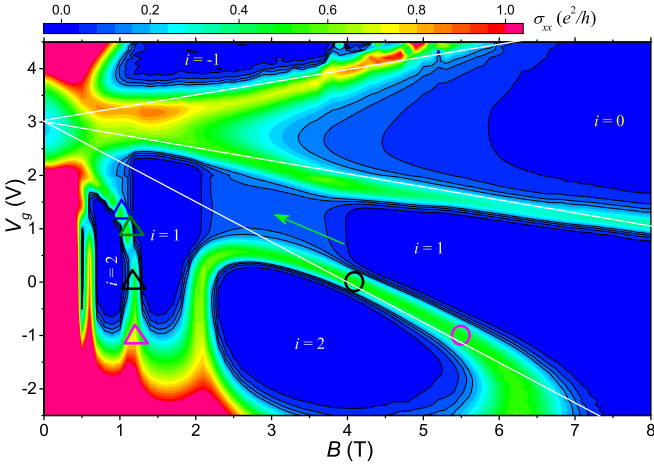


FIG. 5. Color map of the longitudinal conductivity $\sigma_{xx}(B, V_g)$ at $T = 260$ mK. The white lines and the symbols have been reported from Fig. 4. The solid green arrow points toward the σ_{xx} elevation visible around the position of an apparent zero-mode LL anticrossing. The circles and triangles are drawn to compare with similar points in $\sigma_{xy}(B, V_g)$ on Fig. 4(a).

closure, but the local narrowing of the $i = 1$ gap in the anticrossing.

The origin of the anticrossing between the mentioned LLs may be attributed to bulk inversion asymmetry of the unit cell of zinc-blende semiconductors [12,41] or to the interface inversion asymmetry due to anisotropy of chemical bonds at the QW interfaces [42]. The fingerprints of such anticrossings were observed in LL transitions by means of far-infrared magnetic spectroscopy [28,43–46], and a possible impact of many-particle interaction on the observed anticrossings was also discussed [47].

J. RIQHE and anticrossing in the $i = 2$ region

A remarkable modification of the RIQHE has been observed by tilting the magnetic field with respect to the sample normal. As shown in Fig. 6, a tilt angle $\theta > 30^\circ$ suppresses the anomalous peak in $\rho_{yx}(B)$ at the reentrance, so that an extra-long unperturbed flat $i = 2$ plateau appears.

The good reproducibility of the results in the negative field polarity, seen in Fig. 6 both for a perpendicular and a characteristic tilted field, indicates a high quality of the studied samples and the robustness of the observed effects.

The tilt also suppresses the corresponding peak in $\rho_{xx}(B)$, but the complete suppression in this case is at larger tilts $\theta > 44^\circ$, thus indicating a higher sensitivity of $\rho_{xx}(B)$ to the details in the picture of LLs.

Theoretically, the magnetic field component B_{\parallel} parallel to the DQW plane can induce a LL anticrossing even in the absence of interface inversion asymmetry or bulk inversion asymmetry [48]. Based on the symmetry analysis of the 8-band $\mathbf{k} \times \mathbf{p}$ Hamiltonian, we conclude that B_{\parallel} mixes the states of the $n = 1$ and $n = 0$ LLs, thereby opening an anticrossing gap at the expected intersection of these LLs [34]. The implied anticrossing opens an isthmus between the two $i = 2$ regions, so that E_F can now avoid the $i = 1$ region and stay in the continuous $i = 2$ region from low to high magnetic fields.

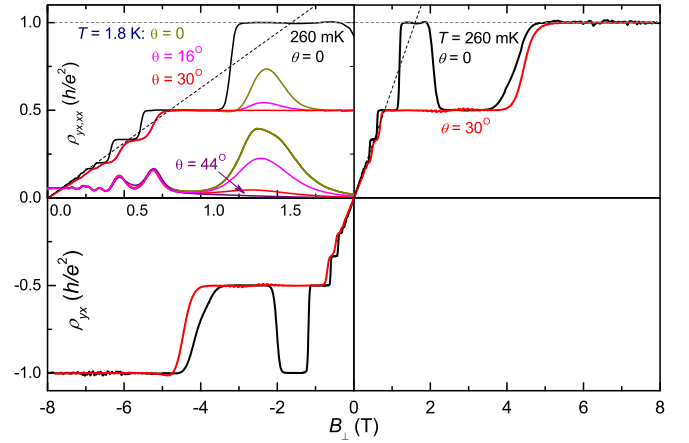


FIG. 6. $\rho_{yx}(B)$ in perpendicular fields (at $T = 260$ mK) and in the rotator (at 1.8 K). The parallel field component suppresses the $i = 1$ state so that a pure flat extra-long $i = 2$ plateau is formed for $\theta > 30^\circ$. The corresponding anomalous peak in $\rho_{xx}(B)$ is fully suppressed for $\theta > 44^\circ$.

Consequently, an undisturbed wide $i = 2$ plateau appears in place of the RIQHE.

K. The missing low-field $i = 0$ gap

A zero filling factor state $i = 0$ is clearly visible at high fields in Figs. 4 and 5. Its divergent triangular shape in the experimental maps is remarkably similar to the shape of the high-field $i = 0$ region formed within the calculated pictures of LLs. This additionally confirms our hierarchy of gap numbering.

This $i = 0$ region collapses at $V_g = +3$ V and $B \approx 2$ T. Randomly, this voltage turns out to be close to the CNP voltage V_{CNP} .

Interestingly, the second $i = 0$ region, which should appear at still lower magnetic fields between the two $n = -2$ LLs according to the calculated picture of LLs in an asymmetric DQW potential, is absent in the experiment. Only in the weakest fields $B \lesssim 0.5$ T does the state $\sigma_{xy} \simeq 0$ reappear on the map, but this area is already close to the transition into the classical mode where the contour lines for fixed values of σ_{xy} on the map must in any case obey the rule $|V_g - V_{\text{CNP}}| \propto 1/B$.

The absence of the $i = 0$ state below the field where the $i = 0$ triangle gap is closed corresponds to the case when the two $n = -2$ LLs coincide; see Fig. 7. In its turn, this indicates that at a sufficiently high gate voltage, around $V_g = +3$ V, the initially asymmetric DQW becomes symmetric.

The above described existence of a gap between the $n = -2$ LLs at high fields, apparent by the observation of the high-field $i = 1$ plateau, Fig. 4(a), and the absence of this gap in weak fields, Fig. 7, can be reconciled by the fact that these two states manifest in our experiment at different V_g , while the asymmetry of the DQW profile is modified by applying a gate voltage. The high-field $i = 1$ plateau connected with this gap is observed at $V_g \leq 0$, while the absence of the $i = 0$ gap is found at $V_g = 3$ V. Thus, just around $V_g = 3$ V the initial DQW asymmetry is compensated by the external electric field due to the applied gate voltage. From rough estimations based on

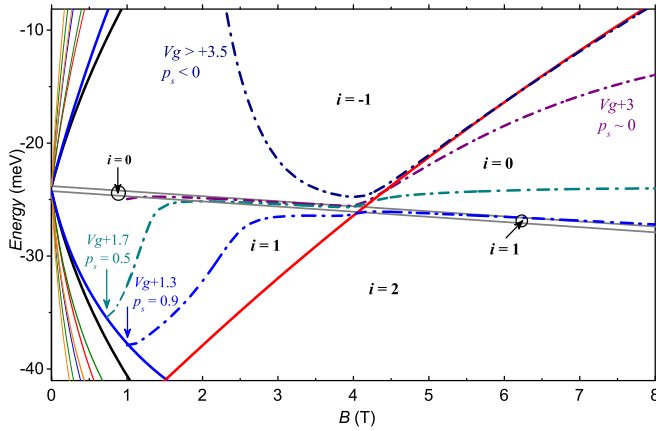


FIG. 7. LL fan chart for a symmetrical DQW with $\mathcal{E} = 0$. The traces of the Fermi level $E_F(B)$ are also reported for four different positive gate voltages that illustrate transitions between different QH states when compared to Fig. 4(a) around CNP at $V_g = +3$ V.

the structure of our gated sample, one expects an electric field variation $\Delta\mathcal{E} \simeq 10$ kV/cm for a gate voltage variation $\Delta V_g \simeq 3$ V. Thus, the experimental data at $V_g = +3$ V and around it should be better analyzed based on Fig. 7 for symmetric DQW while the LL patterns used for other V_g values should contain a gap between the $n = -2$ LLs [these LL patterns may be roughly obtained by interpolations between or extrapolations from Fig. 7 and Fig. 4(b)].

Some difference between the experimental and calculated field positions where the $i = 0$ gap is closed, seen in Fig. 4, could be possibly removed by considering the anticrossing of the upper $n = -2$ LL with the $n = 0$ LL and/or by inclusion of some additional terms into the Hamiltonian. This is an open question which is left for future work.

L. Capacitance estimations above the RIQHE

As we showed above, the transitions $i + 1 \rightarrow i$ at B higher than the RIQHE are driven by the total charge p_s . This implies that V_g and B follow the relation $CV_g = p_s e = (i + 1/2)e^2 B/h$, where C is the geometric capacitance. The relation is shown as white solid lines for $i = 1, 0, -1$ in the $\sigma_{xy}(B, V_g)$ color map, Fig. 4(a), starting at $B = 0$ from the CNP position $V_g = 3$ V, from a single point as we conclude that the DQW randomly becomes symmetric around $V_g = V_{\text{CNP}}$.

Working with the $\sigma_{xy}(B, V_g)$ map, not only the transition $i = 2 \rightarrow 1$ can be analyzed, as described above in weak fields for ρ_{yx} , but also the $i = 0 \rightarrow -1$ and $i = 1 \rightarrow 0$ transitions. These transitions are indeed almost perfectly aligned with the calculated lines, thus confirming the obtained LL pattern and the adequacy of our analysis and gap numbering.

M. Why is RIQHE in DQW?

At first sight, the conditions for observing the RIQHE in DQWs may be realized as well in a single HgTe QW with an inverted spectrum at thicknesses slightly larger than the critical value [26], since it also contains LM, a highly raised topmost hole LL, and an electron-like $n = 0$ LL. However, the differences are (i) the absence of an additional array of

LLs for holes in the central maximum of the second valence subband above the electron-like LL as in a DQW and (ii) that a single topmost hole $n = -2$ LL is in a single QW, not two such LLs as in DQWs. Due to the latter, the corresponding hole filling factors and QH plateau numbers will be shifted one unit down in a single QW with respect to our case. As a result, $E_F(B)$ at relatively high fields will be stabilized near LM in the gap with $i = 1$, not $i = 2$ as in a DQW. That is why the prolonged evolution of $E_F(B)$ from LM to the topmost hole LL with increasing field will be developed within the $i = 1$ gap and, although an extra-long $i = 1$ plateau was really observed in some single HgTe QWs [26,35], this does not give a distinct information on the exhaustion of the LM reservoir. The $i = 1$ QH plateau does not have a distinct high-field boundary, which is dictated by the transition into an insulating state in this case. On the contrary, the high-field boundary of the extended $i = 2$ plateau in the DQW should be distinctly in the vicinity of $i = 1.5$, thus yielding a well-defined value of the total density p_s . The obtained larger value of the latter with respect to the low-field data indicates unambiguously that a reservoir-like phenomenon is implied into the process.

In addition, there is no reason for the reentrant behavior of MR in a single QW, since LLs of only one valence subband are involved in magnetotransport there, whereas in the DQW there is an overlap of downward LLs of the second valence subband ($HH1^1$) and the zero-mode $n = 0$ LL, going up from the first valence subband ($E1^1$) below.

The center part of the DQW energy spectrum resembles the fragments of the bilayer graphene spectrum around K points [49] but the latter has no LM and no anomalous LLs [49,50] to induce the described effects.

V. CONCLUSIONS

In the well-known classical two-fluids model, in which two types of carriers participate in the electrical conductivity, the Hall effect at low field is given by the carriers of highest mobility only, whereas at high magnetic fields, the Hall effect is given by the overall density of both types of carriers. The unconventional QHE observed here can be interpreted as a spectacular quantum extension of this phenomenon. At low magnetic field, a first set of quantum plateaus is initiated only by holes from the central maximum of the valence subband with a small effective mass, while a significant number of holes in the states of the valence subband lateral maximum do not manifest themselves in QHE. At higher fields, a new set of quantum plateaus appears, whose position, shifted to higher fields with respect to the first set, is dictated by the total density of holes. At the transition between the two regimes, the reentrant QHE takes place. A combination of factors is responsible for this remarkable QHE structure: (i) a lateral maximum in the valence subband against the background of the LL fan chart formed from the states of the central maximum, and an achievable proximity of E_F to it in p -type samples; (ii) the existence of two topmost zero-mode hole LLs ($n = -2$) that are significantly raised in energy with respect to the other hole LLs; (iii) a zero-mode electron-like LL ($n = 0$) superposed on LLs of the second subband central maximum.

The observed RIQHE is specific to DQW structures and, presumably, cannot be found in a single p -type HgTe layer

with a Dirac or inverted energy spectrum, even if some similarities are observed [12,26,31,40,46,51].

ACKNOWLEDGMENTS

The authors are grateful to G. M. Minkov and A. A. Sherstobitov for advice on making photolithography and for deposition of the gate. The research was carried out within the state assignment of the RF ministry of science and high education (theme “Electron” No. AAAA-A18-118020190098-5) and its Grant No. 075-15-2020-797 (13.1902.21.0024) (calculations), supported in part by RFBR (trip for measurements to Montpellier: Project No. 18-02-00172, fabrication of the gate: Mol-a No. 18-32-00382 and No. 19-32-50040). The work was partially supported by MIPS department of Montpellier University through the “Occitanie TeraHertz Platform,” by the ANR project “Dirac3D,” by the Occitanie region via the “Gepeto TeraHertz Platform,” and by the CNRS through LIA “TeraMIR.” Some of the measurements were done in the testing center for nanotechnology and advanced materials at M. N. Miheev Institute of Metal Physics UB RAS. We thank S. Gebert for his careful reading of the manuscript and C. Lenhoret for fruitful discussion.

APPENDIX: TWO-FLUID MODEL OF THE MAGNETORESISTIVITY

The observation of a distinct linear part of the classical Hall effect in $\rho_{yx}(B)$ as $B \rightarrow 0$ (Fig. 2), which yields p_s much smaller than the value obtained from QHE at high fields, may be accepted as surprising. To understand this difference, the QHE at low T is compared in Fig. 8 with MR at $T = 30$ K,

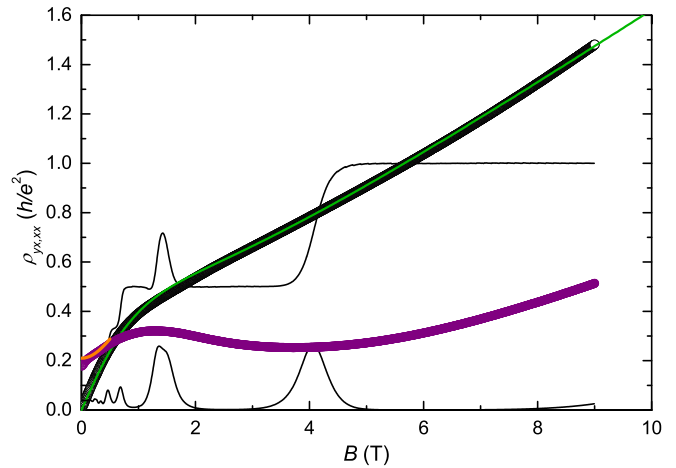


FIG. 8. QHE at 1.8 K and MR at 30 K (circles) with a two-carrier fit for the latter (lines).

when QHE is quenched. At $T = 30$ K, $\rho_{yx}(B)$ also consists of two parts with significantly different slopes, the low-field slope being the same as at low temperatures and the high-field part with much smaller slope crossing the high-field $i = 1$ QH plateau.

This high-temperature $\rho_{yx}(B)$ is reproduced by the so-called classical “two-fluid” model, which takes into account two kinds of holes: a small amount of high-mobility holes, $p_1 = 0.27 \times 10^{15} \text{ m}^{-2}$, $\mu_1 = 3.6 \text{ m}^2/\text{V s}$, and a large density of low-mobility holes, $p_2 = 1.3 \times 10^{15} \text{ m}^{-2}$, $\mu_2 = 0.16 \text{ m}^2/\text{V s}$. These densities are of the same order as those determined from quantum magnetotransport at low temperatures. As seen in Fig. 1 the two kinds of holes may originate from the central valence subband maximum and LM.

- [1] *The Quantum Hall Effect*, 2nd ed., edited by R. E. Prange and S. M. Girvin (Springer-Verlag, New York, 1990).
- [2] X. Y. Lee, H. W. Jiang, and W. J. Schaff, *Phys. Rev. Lett.* **83**, 3701 (1999).
- [3] G. M. Gusev, A. K. Bakarov, T. E. Lamas, and J. C. Portal, *Phys. Rev. Lett.* **99**, 126804 (2007).
- [4] M. P. Lilly, K. B. Cooper, J. P. Eisenstein, L. N. Pfeiffer, and K. W. West, *Phys. Rev. Lett.* **82**, 394 (1999).
- [5] R. R. Du, D. C. Tsui, H. L. Stormer, L. N. Pfeiffer, K. W. Baldwin, and K. W. West, *Solid State Commun.* **109**, 389 (1999).
- [6] K. B. Cooper, M. P. Lilly, J. P. Eisenstein, L. N. Pfeiffer, and K. W. West, *Phys. Rev. B* **60**, R11285 (1999).
- [7] J. P. Eisenstein, K. B. Cooper, L. N. Pfeiffer, and K. W. West, *Phys. Rev. Lett.* **88**, 076801 (2002).
- [8] N. Deng, A. Kumar, M. J. Manfra, L. N. Pfeiffer, K. W. West, and G. A. Csáthy, *Phys. Rev. Lett.* **108**, 086803 (2012).
- [9] E. Kleinbaum, A. Kumar, L. N. Pfeiffer, K. W. West, and G. A. Csáthy, *Phys. Rev. Lett.* **114**, 076801 (2015).
- [10] A. A. Koulakov, M. M. Fogler, and B. I. Shklovskii, *Phys. Rev. Lett.* **76**, 499 (1996).
- [11] M. O. Goerbig, P. Lederer, and C. M. Smith, *Phys. Rev. B* **69**, 115327 (2004).
- [12] M. König, H. Buhmann, L. W. Molenkamp, T. Hughes, C.-X. Liu, X.-L. Qi, and S.-C. Zhang, *J. Phys. Soc. Jpn.* **77**, 031007 (2008).
- [13] M. V. Yakunin, A. V. Suslov, M. R. Popov, E. G. Novik, S. A. Dvoretzky, and N. N. Mikhailov, *Phys. Rev. B* **93**, 085308 (2016).
- [14] S. S. Krishtopenko, W. Knap, and F. Teppe, *Sci. Rep.* **6**, 30755 (2016).
- [15] P. Michetti, J. C. Budich, E. G. Novik, and P. Recher, *Phys. Rev. B* **85**, 125309 (2012).
- [16] P. Michetti and B. Trauzettel, *Appl. Phys. Lett.* **102**, 063503 (2013).
- [17] J. C. Budich, B. Trauzettel, and P. Michetti, *Phys. Rev. Lett.* **112**, 146405 (2014).
- [18] M. V. Yakunin, S. S. Krishtopenko, S. M. Podgornykh, M. R. Popov, V. N. Neverov, N. N. Mikhailov, and S. A. Dvoretzky, *JETP Lett.* **104**, 403 (2016).
- [19] G. M. Gusev, Yu. A. Pusep, A. K. Bakarov, A. I. Toropov, and J. C. Portal, *Phys. Rev. B* **81**, 165302 (2010).
- [20] V. A. Shvets, N. N. Mikhailov, D. G. Ikusov, I. N. Uzhakov, and S. A. Dvoretzky, *Opt. Spectrosc.* **127**, 318 (2019).
- [21] L. S. Bovkun, S. S. Krishtopenko, A. V. Ikonnikov, V. Ya. Aleshkin, A. M. Kadykov, S. Ruffenach, C. Consejo, F. Teppe,

- W. Knap, M. Orlita, B. A. Piot, M. Potemski, N. N. Mikhailov, S. A. Dvoretzki, and V. I. Gavrilenko, *Semiconductors* **50**, 1532 (2016).
- [22] L. S. Bovkun, A. V. Ikonnikov, V. Ya. Aleshkin, S. S. Krishtopenko, N. N. Mikhailov, S. A. Dvoretzki, M. Potemski, B. A. Piot, M. Orlita, and V. I. Gavrilenko, *JETP Lett.* **108**, 329 (2018).
- [23] G. M. Minkov, A. V. Germanenko, O. E. Rut, A. A. Sherstobitov, S. A. Dvoretzki, and N. N. Mikhailov, *Phys. Rev. B* **88**, 155306 (2013).
- [24] G. M. Minkov, A. V. Germanenko, O. E. Rut, A. A. Sherstobitov, M. O. Nestoklon, S. A. Dvoretzki, and N. N. Mikhailov, *Phys. Rev. B* **93**, 155304 (2016).
- [25] A. M. Kadykov, S. S. Krishtopenko, B. Jouault, W. Desrat, W. Knap, S. Ruffenach, C. Consejo, J. Torres, S. V. Morozov, N. N. Mikhailov, S. A. Dvoretzki, and F. Teppe, *Phys. Rev. Lett.* **120**, 086401 (2018).
- [26] I. Yahniuk, S. S. Krishtopenko, Gr. Grabecki, B. Jouault, Ch. Consejo, W. Desrat, M. Majewicz, A. V. Kadykov, K. E. Spirin, V. I. Gavrilenko, N. N. Mikhailov, S. A. Dvoretzki, D. B. But, F. Teppe, J. Wróbel, Gr. Cywiński, S. Kret, T. Dietl, and W. Knap, *npj Quantum Mater.* **4**, 13 (2019).
- [27] L. S. Bovkun, A. V. Ikonnikov, V. Ya. Aleshkin, K. V. Maremyanin, N. N. Mikhailov, S. A. Dvoretzki, S. S. Krishtopenko, F. Teppe, B. A. Piot, M. Potemski, M. Orlita, and V. I. Gavrilenko, *Opto-Electron. Rev.* **27**, 213 (2019).
- [28] M. Orlita, K. Masztalerz, C. Faugeras, M. Potemski, E. G. Novik, C. Brüne, H. Buhmann, and L. W. Molenkamp, *Phys. Rev. B* **83**, 115307 (2011).
- [29] M. Schultz, U. Merkt, A. Sonntag, U. Rössler, R. Winkler, T. Colin, P. Helgesen, T. Skauli, and S. Løvold, *Phys. Rev. B* **57**, 14772 (1998).
- [30] M. J. Schmidt, E. G. Novik, M. Kindermann, and B. Trauzettel, *Phys. Rev. B* **79**, 241306(R) (2009).
- [31] M. König, S. Wiedmann, C. Brüne, A. Roth, H. Buhmann, L. W. Molenkamp, X.-L. Qi, and Sh.-Ch. Zhang, *Science* **318**, 766 (2007).
- [32] A. Hansen, E. H. Hauge, J. Hove, and F. A. Maaø, *Annu. Rev. Comput. Phys.* **5**, 201 (1997).
- [33] E. E. Mendez, L. Esaki, and L. L. Chang, *Phys. Rev. Lett.* **55**, 2216 (1985).
- [34] K. Suzuki, K. Takashina, S. Miyashita, and Y. Hirayama, *Phys. Rev. Lett.* **93**, 016803 (2004).
- [35] W. Zawadzki, A. Raymond, and M. Kubisa, *Phys. Status Solidi B* **251**, 247 (2014).
- [36] S. I. Dorozhkin, *JETP Lett.* **103**, 513 (2016).
- [37] G. A. Baraff and D. C. Tsui, *Phys. Rev. B* **24**, 2274 (1981).
- [38] T. J. B. M. Janssen, A. Tzalenchuk, R. Yakimova, S. Kubatkin, S. Lara-Avila, S. Kopylov, and V. I. Fal'ko, *Phys. Rev. B* **83**, 233402 (2011).
- [39] M. Yang, O. Couturaud, W. Desrat, C. Consejo, D. Kazazis, R. Yakimova, M. Syvajarvi, M. Goiran, J. Beard, P. Frings, M. Pierre, A. Cresti, W. Escoffier, and B. Jouault, *Phys. Rev. Lett.* **117**, 237702 (2016).
- [40] D. A. Kozlov, Z. D. Kvon, N. N. Mikhailov, and S. A. Dvoretzki, *JETP Lett.* **100**, 724 (2014).
- [41] C. Liu, T. L. Hughes, X.-L. Qi, K. Wang, and S.-C. Zhang, *Phys. Rev. Lett.* **100**, 236601 (2008).
- [42] M. V. Durnev and S. A. Tarasenko, *Phys. Rev. B* **93**, 075434 (2016).
- [43] L. S. Bovkun, A. V. Ikonnikov, V. Y. Aleshkin, K. E. Spirin, V. I. Gavrilenko, N. Mikhailov, S. A. Dvoretzki, F. Teppe, B. A. Piot, M. Potemski, and M. Orlita, *J. Phys.: Condens. Matter* **31**, 145501 (2019).
- [44] M. S. Zholudev, F. Teppe, M. Orlita, C. Consejo, J. Torres, N. Dyakonova, M. Czapkiewicz, J. Wróbel, G. Grabecki, N. Mikhailov, S. Dvoretzki, A. Ikonnikov, K. Spirin, V. Aleshkin, V. Gavrilenko, and W. Knap, *Phys. Rev. B* **86**, 205420 (2012).
- [45] M. S. Zholudev, F. Teppe, S. V. Morozov, M. Orlita, C. Consejo, S. Ruffenach, W. Knap, V. I. Gavrilenko, S. A. Dvoretzki, and N. N. Mikhailov, *JETP Lett.* **100**, 790 (2014).
- [46] M. Marcinkiewicz, S. Ruffenach, S. S. Krishtopenko, A. M. Kadykov, C. Consejo, D. B. But, W. Desrat, W. Knap, J. Torres, A. V. Ikonnikov, K. E. Spirin, S. V. Morozov, V. I. Gavrilenko, N. N. Mikhailov, S. A. Dvoretzki, and F. Teppe, *Phys. Rev. B* **96**, 035405 (2017).
- [47] S. S. Krishtopenko, A. M. Kadykov, S. Gebert, S. Ruffenach, C. Consejo, J. Torres, C. Avogadri, B. Jouault, W. Knap, N. N. Mikhailov, S. A. Dvoretzki, and F. Teppe, *Phys. Rev. B* **102**, 041404(R) (2020).
- [48] N. Kumada, K. Iwata, K. Tagashira, Y. Shimoda, K. Muraki, Y. Hirayama, and A. Sawada, *Phys. Rev. B* **77**, 155324 (2008).
- [49] E. McCann and M. Koshino, *Rep. Prog. Phys.* **76**, 056503 (2013).
- [50] F. Mireles and J. Schliemann, *New J. Phys.* **146**, 093026 (2012).
- [51] P. Olbrich, C. Zoth, P. Vierling, K.-M. Dantscher, G. V. Budkin, S. A. Tarasenko, V. V. Bel'kov, D. A. Kozlov, Z. D. Kvon, N. N. Mikhailov, S. A. Dvoretzki, and S. D. Ganichev, *Phys. Rev. B* **87**, 235439 (2013).